IEEE Access
Multidisciplinary ⋮ Rapid Review ⋮ Open Access Journal

Received November 13, 2021, accepted December 5, 2021, date of publication December 10, 2021,
date of current version December 21, 2021.

Digital Object Identifier 10.1109/ACCESS.2021.3134409

A Photonic Dechirp-on-Receive Pulse Synthetic Aperture Radar Using a Phase Correlated Optical Reference Signal in a DSP-Based Optical Coherent Receiver

ZHENWEI MO[1,2], RUOMING LI[1], (Senior Member, IEEE), JIYAO YANG[1,2], CHENYU LIU[1,2], AND WANGZHE LI[1], (Member, IEEE)

[1]National Key Laboratory of Microwave Imaging Technology, Aerospace Information Research Institute, Chinese Academy of Sciences, Beijing 100190, China
[2]School of Electronics, Electrical and Communication Engineering, University of Chinese Academy of Sciences, Beijing 100049, China

Corresponding authors: Ruoming Li (rmli@mail.ie.ac.cn) and Wangzhe Li (wzli@mail.ie.ac.cn)

This work was supported in part by the National Key Research and Development Program of China under Grant 2018YFA0701900 and Grant 2018YFA0701901, and in part by the National Natural Science Foundation of China (NSFC) under Grant 61690191.

ABSTRACT A pulse radar based on photonics-assisted signal generation and stretch processing is proposed and experimentally demonstrated. A radio frequency (RF) linear frequency modulated (LFM) pulse signal is generated by photonic frequency doubling from an intermediate frequency (IF) LFM pulse signal and fed into an antenna for transmitting. An optical reference signal is generated from another coherent IF-LFM pulse signal with an equaled bandwidth and a doubled pulse duration to the transmitted RF-LFM, and the generated optical reference signal is split. The split optical reference signals are separately fed into a polarization and phase diversity coherent receiver (PPDCR) as an optical local oscillation signal (OLO) and a dual-polarization quadrature phase shift keying (DP-QPSK) modulator as an optical carrier. In the DP-QPSK modulator, the input light wave is split into two paths with light wave on one path being intensity-modulated by echoes and light wave on the other path not being modulated. The light waves are polarization orthogonally multiplexed at the output of the DP-QPSK modulator and coherently detected with the OLO in the PPDCR. The information of the echoes can be recovered by using a digital signal processing algorithm from the outputs of the PPDCR. Experiments verify the idea of a photonic dechirp pulse synthetic aperture radar (SAR), which can obtain microwave image with high resolution in a long-range.

INDEX TERMS Photonic signal generation, photonic dechirp-on-receive, pulse synthetic aperture radar, long range, high resolution, microwave imaging.

I. INTRODUCTION

Radar images with continuously enhanced resolution are desired to obtain more information of targets. For a synthetic aperture radar (SAR), the information contained in the Doppler spread of echoes is utilized to improve the azimuth resolution. In range direction, pulse compression technique is employed to decouple the relationship between the resolution and the transmitted power. Radar signals with a large instantaneous bandwidth which is needed for a high range resolution pose challenges to microwave electronic components [1], [2]. Photonic techniques have been studied to enhance the performance of radar systems [3], [4]. A fully photonics-based radar system has been demonstrated [5], and photonic-assisted signal generation and reception have also been studied intensively for SAR systems [6]–[10]. However, as far as we know, the reported high-resolution photonic-assisted SAR systems are based on the dechirp reception in continuous-wave (CW) system. It is well known that the TX/RX isolation of a CW system limits the transmitter output power and thus places a limitation on the maximum detection range. Therefore, the study of photonic dechirp processing based pulse SAR systems is necessary for long-range applications like spaceborne systems.

In the work, the time difference required for a radar signal to return from the near and far edges of the swath is represented by T_s, the duration of the transmitted pulse is represented by T_e, and the duration of the reference pulse

The associate editor coordinating the review of this manuscript and approving it for publication was Muguang Wang.

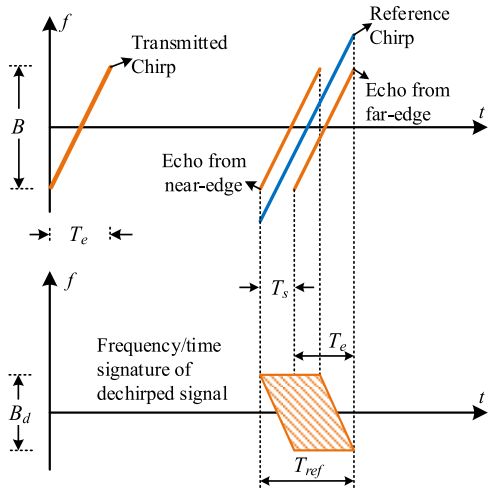

FIGURE 1. Schematic diagram of the time-frequency relationship between a transmitted signal, echoes, a reference signal, and dechirped signals in a dechirp processing based pulse radar system.

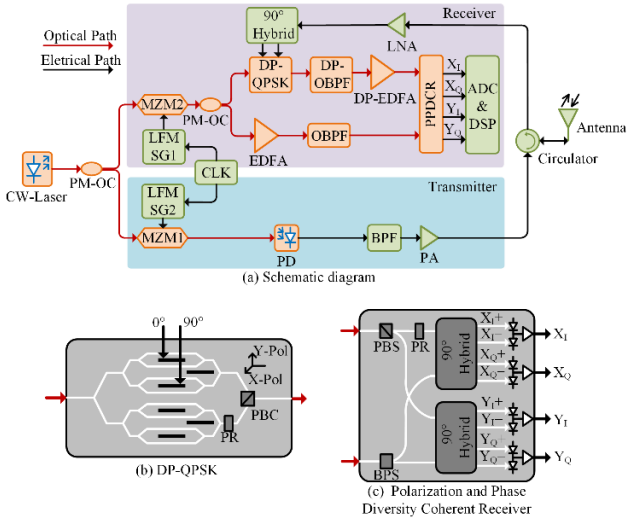

FIGURE 2. (a) Schematic diagram of the proposed photonics-based LFM pulse radar; (b) The structure of the DP-QPSK modulator; (c) The structure of the polarization and phase diversity coherent receiver. CW-Laser, continuous-wave laser; PM-OC, polarization maintaining optical coupler; MZM, Mach-Zehnder modulator; LFM-SG: linear frequency modulated signal generator; CLK: clock source; PD, photodetector; BPF, bandpass filter; LNA, low noise amplifier; PA, power amplifier; EDFA, erbium-doped fiber amplifier; OBPF, optical bandpass filter; DP-QPSK, dual-polarization quadrature phase shift keying modulator; DP-OBPF, dual-polarization optical bandpass filter; DP-EDFA, dual-polarization erbium-doped fiber amplifier; PPDCR, polarization and phase diversity coherent receiver; ADC & DSP, analog-to-digital converter and digital signal processor; PR, polarization rotator; PBC, polarization beam combiner; PBS, polarization beam splitter; BPS, beam power splitter.

is represented by T_{ref}. As shown in Fig.1, for a dechirp-on-receive pulse radar system, T_{ref} should be slightly greater than the summation of T_e and T_s such that the resolution implied by the transmitted signal bandwidth can be obtained by processing the complete LFM pulses reflected by the near and far edges of the swath [11]. As a result, unlike the previous photonic-assisted SAR systems operating in CW mode, the receiver in the photonic dechirp processing based pulse radar system should offer a reference signal different from the transmitted signal. Since the chirp rate of the transmitted and reference are the same, the requirement also means a greater bandwidth for the reference signal, which raises a challenge to the electronic components in the reference path [6], [10].

In this paper, a dechirp reception based photonic pulse radar system is proposed. In the transmitter, a transmitted LFM pulse signal with a pulse duty-cycle of 10% is generated by photonic frequency doubling from an intermediate frequency (IF) LFM pulse. In the receiver, instead of using a RF reference signal with a doubled duration and bandwidth to the transmitted signal, an optical reference signal is generated by modulating a CW light wave with another coherent IF-LFM pulse signal which has a doubled duration and an equaled bandwidth to the transmitted signal on a Mach-Zehnder modulator (MZM). As a result, the maximum bandwidth of all RF signals in the system is reduced to the bandwidth of transmitted RF signal, which mitigates the requirement on the analog RF components in the reference path. After that, the optical reference signal is split into two paths. One of the split optical reference signals is applied as an optical local oscillation (OLO) and directly coupled to a polarization and phase diversity coherent receiver (PPDCR). The other path is coupled to a dual-polarization quadrature phase shift keying (DP-QPSK) modulator to generate an orthogonally polarization multiplexed optical signal with the light wave on one polarization being intensity-modulated by echoes and the light wave on the other polarization not being modulated. In the PPDCR, the orthogonally polarized optical signal is coherent detected with the OLO. The beating results of the echo modulated light wave and the OLO provide the information of targets, the information of path difference between the OLO and the orthogonally polarized optical signal, and a phase noise which is introduced by the statistical fluctuations of the refractive index of an optical medium at a temperature above absolute zero [12], [13]. The beating result of the non-modulated light wave and the OLO also contains the information of the path difference, and the phase noise due to thermodynamic temperature fluctuations. Since the orthogonally polarization multiplexed optical signal are traveling in the same optical path, the relative phase variations between the light on two polarizations due to the thermodynamic fluctuations are very small [14], [15]. The dechirped results can be recovered by using a digital signal processing algorithm to cancel the common phase noise of optical fiber.

A pulse radar system with the proposed dechirp reception method is experimentally demonstrated. The radar operates in Ku band with a bandwidth of 2GHz, a signal repetition time of 100us, and a duty-cycle of 10%. The performance of the experimental radar is evaluated through a series of experiments.

II. PRINCIPLE

Fig. 2 shows the schematic diagram of the proposed dechirp reception based photonic pulse radar. A CW light from the

CW-Laser is equally split into two paths by a polarization-maintaining optical coupler (PM-OC). In the transmitter path, the light wave is modulated by an IF-LFM signal on a Mach-Zehnder modulator (MZM1). The IF-LFM signal is generated by an electronic signal generator and is expressed as:

$$S_{IF-T}(t) = \sum_{n=1}^{N} rect\left(\frac{t-nPRI}{T_e}\right) V_e \times \cos\left[\begin{matrix}\pi f_c (t-nPRI)+ \\ \frac{k}{2}\pi (t-nPRI)^2\end{matrix}\right],$$
$$rect\left(\frac{t-nPRI}{T_e}\right) = \begin{cases} 1, & 0 < t-nPRI \le T_e \\ 0, & else \end{cases} \quad (1)$$

where T_e is the pulse duration, V_e is the amplitude, f_c is the initial frequency, k is the chirp rate of the transmitted pulse signal, PRI is the pulse repetition interval of the transmitted pulse, and $n = 0, 1, 2, \ldots, N$ denotes the $(n+1)$th transmitted period. For the simplicity of the expressions, only one period of the transmitted signal, which $n = 0$, is considered in the following derivation. The MZM1 is biased at the minimum transmission point (MITP) to suppress the optical carrier and the even-order sidebands. The modulation index can be set that only the ± 1st order sidebands have significant values [16], [17].

The output of the MZM1 can be expressed as:

$$E_{MZM1}(t) = -rect(t/T_e) A_0 \exp\left(j2\pi f_0 t + j\frac{\pi}{2}\right) \times \left\{\begin{matrix} J_1(\beta_e)\exp\left[-j\left(\pi f_c t + \frac{k}{2}\pi t^2\right)\right] \\ +J_1(\beta_e)\exp\left[j\left(\pi f_c t + \frac{k}{2}\pi t^2\right)\right]\end{matrix}\right\} \quad (2)$$

where A_0 and f_0 are the electric field amplitude and the frequency of the light from the CW-Laser, J_1 denotes the first order of the Bessel function of the first kind, $\beta_e = V_e\pi/V_\pi$ is the modulation index, and V_π is the half-wave voltage. The output of the MZM1 is then fed into a photodetector (PD) to generate the frequency doubled RF-LFM signal, which is expressed as:

$$S_e(t) = R|E_{MZM1}(t)|^2 = 2rect(t/T_e) RA_0^2 J_1(\beta_e)^2\left[1+\cos\left(2\pi f_c t + k\pi t^2\right)\right] \quad (3)$$

where R denotes the responsibility of the PD. After passing a RF bandpass filter (BPF), an LFM pulse radar signal with doubled carrier frequency and bandwidth is obtained. Then the generated signal is amplified by a power amplifier (PA) and radiated by an antenna via a circulator.

In the receiver path, the light wave is coupled to the MZM2 and modulated by an electrical IF-LFM reference signal. Since the sample clock of the two IF-LFM generators are locked to a common clock source, as shown in Fig.2, the IF-LFM reference signal is coherent to the radar transmitted signal. The IF-LFM reference signal is expressed as:

$$S_{IF-REF}(t) = rect\left(\frac{t-\tau_0}{T_{ref}}\right) V_{ref} \times \cos\left[\pi f_c (t-\tau_0) + \frac{k}{2}\pi (t-\tau_0)^2\right] \quad (4)$$

where $T_{ref} = T_e + T_s$ is the pulse duration of the reference pulse, V_{ref} is the amplitude, and τ_0 is the reference delay setting by the IF-LFM generators according to the range from the radar to the center of the swath.

The MZM2 is also biased at MITP, and the output of the MZM2 is written as:

$$E_{MZM2}(t) = -rect\left(\frac{t-\tau_0}{T_{ref}}\right) A_0 \exp\left[j2\pi f_0 (t-\tau_0) + j\frac{\pi}{2}\right] \times \left\{\begin{matrix} J_1(\beta_{ref})\exp\left\{-j\left[\pi f_c (t-\tau_0) + \frac{k}{2}\pi (t-\tau_0)^2\right]\right\} \\ +J_1(\beta_{ref})\exp\left\{j\left[\pi f_c (t-\tau_0) + \frac{k}{2}\pi (t-\tau_0)^2\right]\right\}\end{matrix}\right\} \quad (5)$$

where $\beta_{ref} = V_{ref}\pi/V_\pi$ is the modulation index of the reference pulse. The modulated optical signal is split into two paths by a PM-OC. The light wave in one path is sent to a DP-QPSK that comprises a polarization rotator (PR), a polarization beam combiner (PBC), and two QPSK modulators each of which is composed of two sub-MZMs as shown in Fig. 2(b). The light wave fed into one of the QPSK modulators is not modulated, while the light wave fed into another QPSK modulator is carrier suppressed single sideband (CS-SSB) modulated by echoes. To achieve CS-SSB modulation, the echoes first pass an 90° RF hybrid coupler to obtain quadrature signals which are respectively applied to drive the two sub-MZMs of the QPSK, and the bias of the QPSK is set to ensure the phase difference between the output lights of the two sub-MZMs is $|\pi/2|$. At the output of the DP-QPSK modulator, the output of the two QPSKs are polarization multiplexed, and can be expressed as (6), shown at the bottom of the next page, where $E_X(t)$ and $E_Y(t)$ denote the electrical fields of the light wave in orthogonal polarizations of the output of the DP-QPSK, $\beta_{echo} = V_{echo}\pi/V_\pi$, and τ_r is the round trip time from radar to target. As mentioned above, to obtain the range resolution implied by the bandwidth of the transmitted signal, an echo with a time delay of τ_r should satisfy the condition of $\tau_0 \le \tau_r \le \tau_0 + T_{ref} - T_e$. The orthogonally polarized optical signals are fed into a dual-polarization optical bandpass filter (DP-OBPF) to select the useful optical sidebands, and the output signals of the filter are amplified by a dual-polarization erbium-doped fiber amplifier (DP-EDFA). The output of the DP-EDFA can be expressed as (7), shown at the bottom of the next page, where g_1 is the gain of the DP-EDFA. The amplified orthogonally polarized optical signals are then sent into the PPDCR.

The light wave from the other output of the PM-OC is amplified by an EDFA and passes through an OBPF to select the +1st order sideband of the output of MZM2. The selected optical signal is used as the OLO of the PPDCR and expressed as:

$$\begin{aligned} &E_{LO}(t) \\ &= -\frac{\sqrt{2}}{2} rect\left(\frac{t-\tau_0-\tau_d}{T_{ref}}\right) g_2 A_0 J_1\left(\beta_{ref}\right) \\ &\quad \times \exp\left[j\left(\begin{array}{c} 2\pi f_0\left(t-\tau_0-\tau_d\right)+\pi f_c\left(t-\tau_0-\tau_d\right) \\ +\frac{k}{2}\pi\left(t-\tau_0-\tau_d\right)^2+\varphi(t)+\frac{\pi}{2} \end{array}\right)\right] \end{aligned} \tag{8}$$

where g_2 is the gain of the EDFA, τ_d is the transmission time difference of the light waves introduced by the length difference between the optical paths of the polarization multiplexed signal and the OLO, $\varphi(t)$ is the phase noise of optical fiber due to thermal fluctuations along the two optical paths.

As shown in Fig. 2(c), in the PPDCR, the polarization multiplexed signal is polarization split, and then the split signals are coherently detected with the OLO independently [18]. The outputs of the PPDCR are expressed (9), shown at the bottom of the page and (10)–(12), shown at the bottom of the next page.

The outputs of the I and Q channels of the PPDCR can be used to form complex signals (13) and (14), shown at the bottom of the next page.

The phase noise of optical fiber $\phi(t)$ can be canceled by performing:

$$\begin{aligned} K_{XY}(t) &= S_X(t)/S_Y(t) \\ &= 2rect\left(\frac{t-\tau_r}{T_e}\right) J_1\left(\beta_{echo}\right) \\ &\quad \times \exp\left\{j\left[2k\pi\left(\tau_r-\tau_0\right)t+2\pi f_c\left(\tau_r-\tau_0\right)\right.\right. \\ &\qquad \left.\left.-k\pi\left(\tau_r^2-\tau_0^2\right)+\frac{\pi}{2}\right]\right\} \end{aligned} \tag{15}$$

From (15), the phase noise $\varphi(t)$ is canceled while the information of the target is preserved. The obtained signal $K_{XY}(t)$ can be further processed for imaging.

III. EXPERIMENT AND RESULT

To evaluate the performance of the proposed radar system, an experimental photonic radar system is built based on

$$\begin{aligned} \begin{bmatrix} E_X(t) \\ E_Y(t) \end{bmatrix} &= \begin{bmatrix} \frac{1}{4}E_{MZM2}(t)\, rect\left(\frac{t-\tau_r}{T_e}\right)\left\{\begin{array}{l} \exp\left\{j\left[\beta_{echo}\cos\left[2\pi f_c\left(t-\tau_r\right)+k\pi\left(t-\tau_r\right)^2\right]+\pi\right]\right\}+\exp\left\{j\left[-\beta_{echo}\cos\left[2\pi f_c\left(t-\tau_r\right)+k\pi\left(t-\tau_r\right)^2\right]\right]\right\} \\ +(-j)\exp\left\{j\left[\beta_{echo}\cos\left[2\pi f_c\left(t-\tau_r\right)+k\pi\left(t-\tau_r\right)^2+\frac{\pi}{2}\right]+\pi\right]\right\}+(-j)\exp\left\{j\left[-\beta_{echo}\cos\left[2\pi f_c\left(t-\tau_r\right)+k\pi\left(t-\tau_r\right)^2+\frac{\pi}{2}\right]\right]\right\} \end{array}\right\} \\ \frac{1}{2}E_{MZM2}(t) \end{bmatrix} \\ &= \begin{bmatrix} \frac{1}{2}jE_{MZM2}(t)\, rect\left(\frac{t-\tau_r}{T_e}\right)\left\{\begin{array}{l} \sum\limits_{n=-\infty}^{\infty}(-1)^n J_{2n-1}\left(\beta_{echo}\right)\exp\left\{j(2n-1)\left[2\pi f_c\left(t-\tau_r\right)+k\pi\left(t-\tau_r\right)^2\right]\right\} \\ -j\sum\limits_{n=-\infty}^{\infty}(-1)^n J_{2n-1}\left(\beta_{echo}\right)\exp\left\{j(2n-1)\left[2\pi f_c\left(t-\tau_r\right)+k\pi\left(t-\tau_r\right)^2+\frac{\pi}{2}\right]\right\} \end{array}\right\} \\ \frac{1}{2}E_{MZM2}(t) \end{bmatrix} \\ &\approx -rect\left(\frac{t-\tau_0}{T_{ref}}\right) A_0 J_1\left(\beta_{ref}\right)\exp\left[j2\pi f_0\left(t-\tau_0\right)\right] \\ &\quad \times \begin{bmatrix} rect\left(\frac{t-\tau_r}{T_e}\right) J_1\left(\beta_{echo}\right)\left\{\begin{array}{l} \exp\left[j\left(2\pi f_c\left(t-\tau_r\right)+k\pi\left(t-\tau_r\right)^2-\pi f_c\left(t-\tau_0\right)-\frac{k}{2}\pi\left(t-\tau_0\right)^2\right)\right] \\ +\exp\left[j\left(2\pi f_c\left(t-\tau_r\right)+k\pi\left(t-\tau_r\right)^2+\pi f_c\left(t-\tau_0\right)+\frac{k}{2}\pi\left(t-\tau_0\right)^2\right)\right] \end{array}\right\} \\ \frac{j}{2}\left\{\exp\left\{-j\left[\pi f_c\left(t-\tau_0\right)+\frac{k}{2}\pi\left(t-\tau_0\right)^2\right]\right\}+\exp\left\{j\left[\pi f_c\left(t-\tau_0\right)+\frac{k}{2}\pi\left(t-\tau_0\right)^2\right]\right\}\right\} \end{bmatrix} \end{aligned} \tag{6}$$

$$\begin{aligned} \begin{bmatrix} E_X(t) \\ E_Y(t) \end{bmatrix} &= -rect\left(\frac{t-\tau_0}{T_{ref}}\right) g_1 A_0 J_1\left(\beta_{ref}\right)\exp\left[j2\pi f_0\left(t-\tau_0\right)\right] \\ &\quad \times \begin{bmatrix} rect\left(\frac{t-\tau_r}{T_e}\right) J_1\left(\beta_{echo}\right)\exp\left\{j\left[\begin{array}{l} 2\pi f_c\left(t-\tau_r\right)+k\pi\left(t-\tau_r\right)^2- \\ \pi f_c\left(t-\tau_0\right)-\frac{k}{2}\pi\left(t-\tau_0\right)^2 \end{array}\right]\right\} \\ \frac{1}{2}\exp\left\{j\left[\pi f_c\left(t-\tau_0\right)+\frac{k}{2}\pi\left(t-\tau_0\right)^2+\frac{\pi}{2}\right]\right\} \end{bmatrix} \end{aligned} \tag{7}$$

$$\begin{aligned} X_I(t) &= \frac{\sqrt{2}R}{4} rect\left(\frac{t-\tau_0}{T_{ref}}\right) rect\left(\frac{t-\tau_r}{T_e}\right) rect\left(\frac{t-\tau_0-\tau_d}{T_{ref}}\right) \\ &\quad \times g_1 g_2 A_0^2 J_1^2\left(\beta_{ref}\right) J_1\left(\beta_{echo}\right) \\ &\quad \times \cos\left[\begin{array}{l} k\pi\left(2\tau_r-2\tau_0-\tau_d\right)t+\pi f_c\left(2\tau_r-2\tau_0-\tau_d\right) \\ +\frac{k}{2}\pi\left(2\tau_0^2-2\tau_r^2+\tau_d^2\right)+k\pi\tau_0\tau_d-2\pi f_0\tau_d+\varphi(t)+\frac{\pi}{2} \end{array}\right] \end{aligned} \tag{9}$$

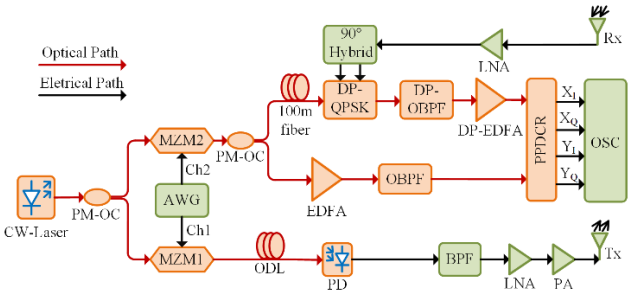

FIGURE 3. The experimental setup of the proposed radar system. AWG: arbitrary waveform generator; ODL: optical delay line; OSC: oscilloscope.

Fig. 3. Limited by available components in the laboratory, instead of using a microwave circulator and an antenna, a pair of horn antennas are employed in the experimental setup. A light wave at 1550nm with a power of 18dBm from a CW-laser (Teraxion, narrow linewidth laser) is split into two paths by a 50:50 PM- OC. Two coherent IF-LFM signals are generated by a dual-channel arbitrary waveform generator (AWG) (Keysight, M8190A) which has a sampling rate of 12GSa/s for each channel. In the experiment, the output format of the DAC of the AWG is doublet and signals at the second Nyquist region are selected to obtain signals with a frequency higher than 6GHz [19]. The IF transmitted signal has a frequency span of 7GHz to 8GHz, a pulse duration of 10μs, and a signal repetition time of 100μs. Meanwhile, the generated IF reference signal has a frequency span of 7GHz to 9GHz, a pulse duration of 20μs and a signal repetition time of 100μs respectively. The frequency spectrum of the IF reference signal is shown in Fig. 4(a). In the transmitter path, the split light wave is sent to the MZM1 and modulated by the IF transmitted signal. An optical delay line (ODL) is employed between the MZM1 and the PD to simulate the time delay of the echoes in the delay test. After optical-to-electrical conversion by a PD (Discovery Semiconductors, DSC20H), a frequency doubling transmitted signal with a bandwidth of 2GHz and a central frequency of 15GHz is generated. The spectrum of the transmitted signal is shown in Fig. 4(b).

In the receiver path, the light wave is modulated on the MZM2 by the IF reference signal. Then the modulated light wave is split into two paths by another 50:50 PM-OC. One

$$\begin{aligned} X_Q(t) = {} & \frac{\sqrt{2}R}{4} rect\left(\frac{t-\tau_0}{T_{ref}}\right) rect\left(\frac{t-\tau_r}{T_e}\right) rect\left(\frac{t-\tau_0-\tau_d}{T_{ref}}\right) \\ & \times g_1 g_2 A_0^2 J_1^2\left(\beta_{ref}\right) J_1\left(\beta_{echo}\right) \\ & \times \sin\left[\begin{array}{l} k\pi\left(2\tau_r-2\tau_0-\tau_d\right)t+\pi f_c\left(2\tau_r-2\tau_0-\tau_d\right) \\ +\frac{k}{2}\pi\left(2\tau_0^2-2\tau_r^2+\tau_d^2\right)+k\pi\tau_0\tau_d-2\pi f_0\tau_d+\varphi(t)+\frac{\pi}{2} \end{array}\right] \end{aligned} \tag{10}$$

$$\begin{aligned} Y_I(t) = {} & \frac{\sqrt{2}R}{8} rect\left(\frac{t-\tau_0}{T_{ref}}\right) rect\left(\frac{t-\tau_0-\tau_d}{T_{ref}}\right) g_1 g_2 A_0^2 J_1^2\left(\beta_{ref}\right) \\ & \times \cos\left[-k\pi\tau_d t+k\pi\tau_d\tau_0-\pi\left(f_c+2f_0\right)\tau_d+\frac{k}{2}\pi\tau_d^2+\varphi(t)\right] \end{aligned} \tag{11}$$

$$\begin{aligned} Y_Q(t) = {} & \frac{\sqrt{2}R}{8} rect\left(\frac{t-\tau_0}{T_{ref}}\right) rect\left(\frac{t-\tau_0-\tau_d}{T_{ref}}\right) g_1 g_2 A_0^2 J_1^2\left(\beta_{ref}\right) \\ & \times \sin\left[-k\pi\tau_d t+k\pi\tau_d\tau_0-\pi\left(f_c+2f_0\right)\tau_d+\frac{k}{2}\pi\tau_d^2+\varphi(t)\right] \end{aligned} \tag{12}$$

$$\begin{aligned} S_X(t) \equiv {} & X_I(t)+jX_Q(t) \\ = {} & \frac{\sqrt{2}R}{4} rect\left(\frac{t-\tau_0}{T_{ref}}\right) rect\left(\frac{t-\tau_r}{T_e}\right) rect\left(\frac{t-\tau_0-\tau_d}{T_{ref}}\right) \\ & \times g_1 g_2 A_0^2 J_1^2\left(\beta_{ref}\right) J_1\left(\beta_{echo}\right) \\ & \times \exp\left\{j\left[\begin{array}{l} k\pi\left(2\tau_r-2\tau_0-\tau_d\right)t+\pi f_c\left(2\tau_r-2\tau_0-\tau_d\right) \\ +\frac{k}{2}\pi\left(2\tau_0^2-2\tau_r^2+\tau_d^2\right)+k\pi\tau_0\tau_d-2\pi f_0\tau_d+\varphi(t)+\frac{\pi}{2} \end{array}\right]\right\} \end{aligned} \tag{13}$$

$$\begin{aligned} S_Y(t) \equiv {} & Y_I(t)+jY_Q(t) \\ = {} & \frac{\sqrt{2}R}{8} rect\left(\frac{t-\tau_0}{T_{ref}}\right) rect\left(\frac{t-\tau_0-\tau_d}{T_{ref}}\right) g_1 g_2 A_0^2 J_1^2\left(\beta_{ref}\right) \\ & \times \exp\left\{j\left[-k\pi\tau_d t+k\pi\tau_d\tau_0-\pi\left(f_c+2f_0\right)\tau_d+\frac{k}{2}\pi\tau_d^2+\varphi(t)\right]\right\} \end{aligned} \tag{14}$$

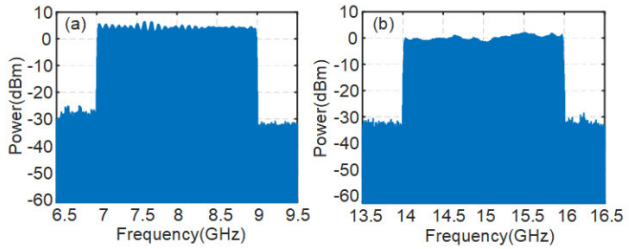

FIGURE 4. (a) The RF spectrum of the IF-reference signal, (b) The RF spectrum of the transmitted signal.

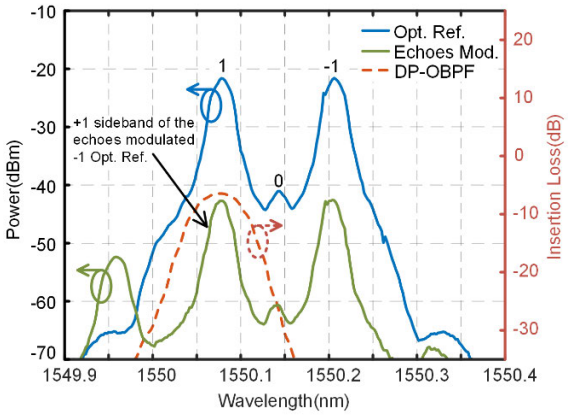

FIGURE 5. The transmission spectrum of the DP-OBPF; The optical spectra of the optical reference signal and the echoes modulated signal. Opt. Ref.: optical reference signal; Echoes Mod.: echoes modulated signal.

path is sent to an off-the-shelf PPDCR (Discovery Semiconductors, R413) as the OLO via an EDFA and an OBPF which selects the +1st order optical sideband. The other path is sent to a DP-QPSK modulator via a 100m polarization-maintaining (PM) fiber which is used to increase fiber phase noise due to thermodynamic temperature fluctuations. In the DP-QPSK modulator, the optical reference signal is split into two paths and sent to two QPSK modulators respectively. One QPSK modulator works in the CS-SSB mode, and the optical reference signal is modulated by the echoes. Note that, the +1st order sideband at the output of the QPSK is generated by modulating the −1st order sideband of the optical reference signal by the echoes. In the other QPSK modulator, two sub-MZM are biased at the peak point, and the optical reference signal is not modulated. A bias controller (PlugTech, MBC-DPIQ-02) is used to ensure the bias state of the DP-QPSK is stable in the experiment. The outputs of the two QPSKs are polarization orthogonally multiplexed at the output of the DP-QPSK. The optical spectra of the orthogonally polarized optical signals are shown in Fig. 5. The +1st order sidebands of the orthogonally polarized optical signals are selected by the DP-OBPF and amplified by the DP-EDFA. In the PPDCR, the orthogonally polarized optical signals are coherently detected with the OLO signal, and the four outputs of the PPDCR are sampled by a four channels oscilloscope (Keysight, DSO-X 92004A) with a sample rate of 40GSa/s. The PPDCR has the maximum

TABLE 1. The calculated results of IRW, PSLR and ISLR.

	Without phase noise cancellation [a]				With phase noise cancellation [b]				In theory[c]
ODL (m)	200	400	1200	2000	200	400	1200	2000	-
IRW (kHz)	90	90	90	90	90	90	90	90	89
PSLR (dB)	−10.64	−11.02	−11.41	−13.10	−11.98	−12.09	−12.36	−12.11	−13.26
ISLR[d] (dB)	−7.12	−5.57	−7.04	−7.07	−9.35	−9.49	−8.82	−9.45	−9.79

[a]The results are calculated from the dechirped signals without phase variation cancellation which are shown in Fig. 6(e)-(h).
[b]The results are calculated from the dechirped signals with phase variation cancellation which are shown in Fig. 6(i)-(l).
[c]The theoretical values are numerical calculated by the ideal LFM signal with the same signal parameters set in the experiment.
[d]The ISLRs are calculated by integrating the sidelobe power within a frequency span of ±3MHz around the peak.

allowed input power of 0dBm at its signal input port and 16dBm at its OLO input port. Thus, it is possible to further enhance the output RF power by enhancing the OLO power.

To verify the basic T/R operation of the radar, a delay line test is performed. By changing the length of the ODL, the delay time of the echo τ_r is changed. As mentioned in the section of principle, when τ_r is tuned within the range of $T_{ref} - T_e$, the range resolution of the radar is not deteriorated. In the experiment, the difference between the pulse durations of the reference signal and the transmitted signal is 10μs which is equivalent to a fiber length about 2045m. Thus, a series of single mode fibers with lengths of 200m, 400m, 1200m and 2000m are used as the ODL in the experiment to observe the variation of the range resolution. The waveform of the transmitted signals with different time delays and the reference signals are shown in Fig. 6(a)-(d). It can be seen that the duration of the reference signal is larger than the transmitted signal. The frequency spectrum of the dechirped results at the X_I output of the PPDCR are shown in Fig. 6(e)-(h) while the corresponded results after fiber phase noise cancellation are shown in Fig. 6(i)-(l).

The peaks of the spectra in Fig. 6(i)-(l) has a frequency shift of 51.82MHz compared to the peaks of the spectra in Fig. 6(e)-(h). The frequency shift is caused by the cancellation of path difference between the polarization multiplexed signal path and the OLO. The path difference can be converted to time difference by $\tau_d = 2f_{\text{shift}}/k$, where f_{shift} is the frequency shift and k is the chirp rate of the transmitted signal. The calculated τ_d is 0.51μs, which is close to the time delay brought by a section of 100m fiber inserted in the polarization multiplexed signal path in the experiment.

Table 1 shows the calculated results of the impulse response width (IRW), peak-to-sidelobe ratio (PSLR), and the integrated sidelobe ratio (ISLR) of the dechirped results shown in Fig. 6(e)-(l). IRW is an indicator to evaluate the radar range resolution while PSLR and ISLR are indicators to evaluate the sidelobe energy distribution which is important for SAR application [20]. As shown in Table 1, the IRWs

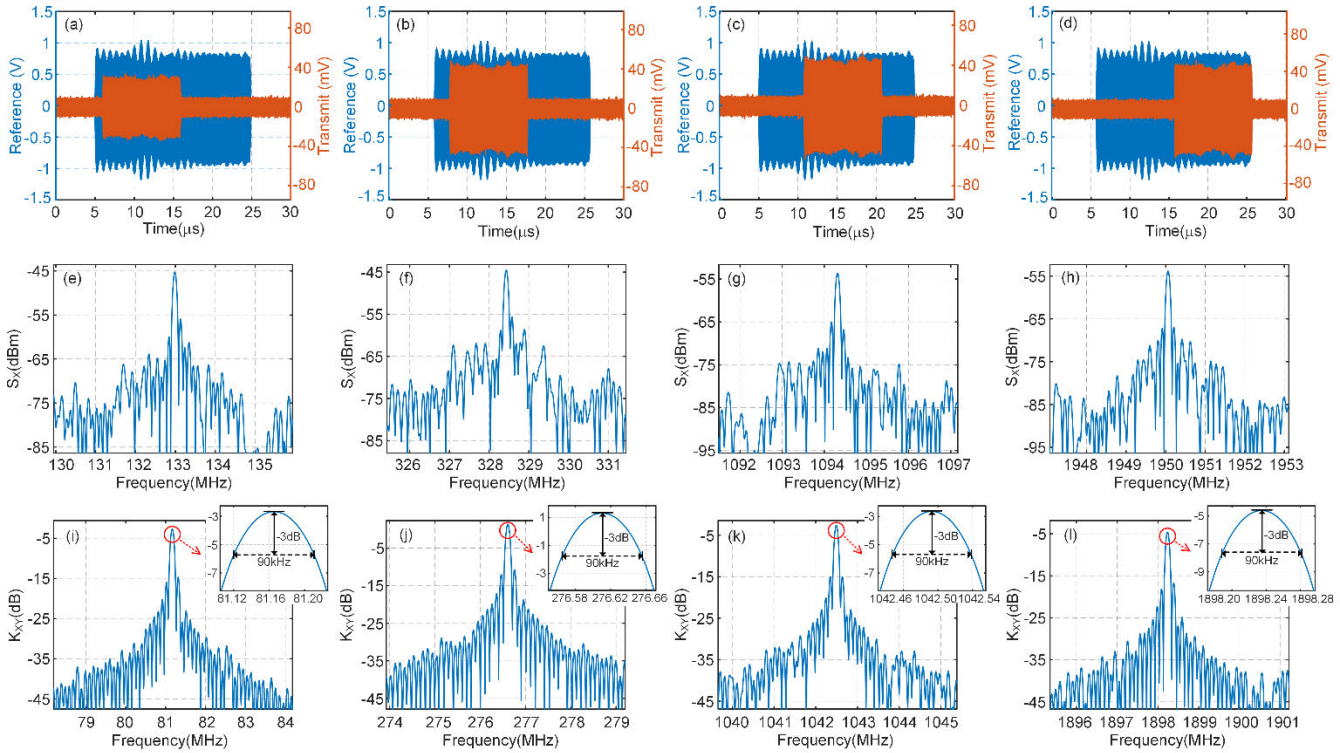

FIGURE 6. (a)-(d): The waveforms of the reference signal and the transmitted signal in the tunable delay line test. (e)-(h): The frequency spectra of the output waveform at X_I port of the PPDCR. (i)-(l): The frequency spectra of the dechirped results after fiber phase noise cancellation. ODL length: (a)(e)(i) 200m; (b)(f)(j) 400m; (c)(g)(k) 1200m; (d)(h)(l) 2000m.

of the dechirped results remain 90kHz under different ODL lengths with or without phase noise cancellation, and it is close to the ideally numerical calculated IRW of 89kHz. The range resolution ΔR can be obtained by frequency to distance conversion with $\Delta R = c\Delta f/2k$, where Δf is the IRW in the frequency domain. The range resolution is 6.7cm calculated with the IRW of 90kHz in the experiment and matches well with the theoretical value of 6.6cm calculated by $0.886c/2B$, where B is the bandwidth of the transmitted signal [20].

Moreover, compared to the spectra of the dechirped results without post-processing that shown in Fig. 6(e)-(h), the spectra of the dechirped results with the phase noise cancellation in (15) that shown in Fig. 6(i)-(l) are closer to the ideal profile which is a Sinc or sin(x)/x. As shown in Table 1, the phase noise cancellation brings no significant improvement to the PSLRs, but the ISLRs with phase noise cancellation are apparently enhanced and are closer to the ideally ISLR. The delay line test confirms that the pulses are being transmitted and received well. The constant radar resolution that is close to the theoretical resolution verifies that the complete echoes reflected from different ranges within the swath is dechirp processed by the reference signal. Furthermore, using the fiber phase noise cancellation, a better pulse compression result can be obtained.

To verify pulse-to-pulse coherence and azimuth compression, an inverse synthetic aperture radar (ISAR) test with the targets of two trihedral corner reflectors(TCRs)on the rotating platform is performed. The sample rate of the oscilloscope

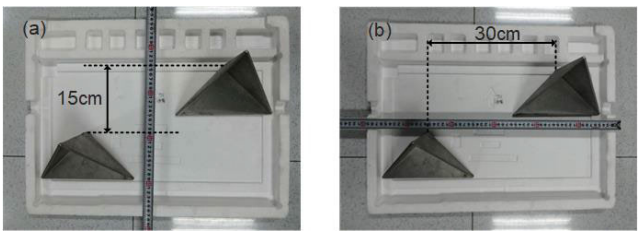

FIGURE 7. The placement of the two TCRs. (a) The initial range distance of the two TCRs; (b) The initial cross-range distance of the two TCRs.

is set to 1GSa/s in the experiment. ODLs with lengths of 200m and 400m are used to tune the delay of the transmitted signal to simulate echoes from different distances. As shown in Fig. 7, the initial range distance and the initial cross-range distance of the two TCRs are 15cm and 30cm respectively.

In the experiment, the two TCRs are placed on a rotation platform, and the rotating speed is 30degree/s. The ISAR imaging coherent integration time is 0.2s. The ISAR imaging results with different fiber lengths and different processing are shown in Fig. 8(a)-(d). Comparing Fig. 8(b)(d) with Fig. 8(a)(c), the ISAR images after phase noise cancellation by (15) have a better performance in terms of focusing and sidelobes distribution in both range and azimuth directions. Note that, a few strong scattering points can be found in the Fig. 8(a)(b), which is attributed to effect of multireflection between two TCRs. The range difference between the results with and without phase cancellation is caused by the length

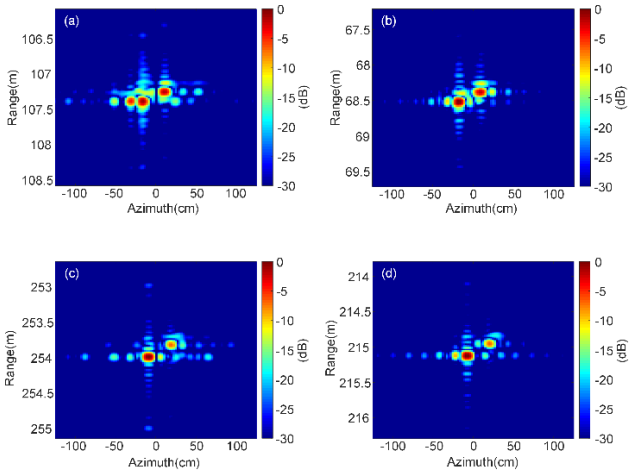

FIGURE 8. **The ISAR images of the two TCRs when the ODL is applied to simulate long distance target. (a): 200m without phase noise cancellation; (b): 200m with phase noise cancellation; (c): 400m without phase noise cancellation; (d): 400m with phase noise cancellation.**

difference between the paths of the polarization multiplexed signal and the OLO as mentioned above. These results verify that the radar data is coherent from pulse to pulse, and the proposed system can produce properly focused targets.

IV. CONCLUSION

In this paper, a configuration of photonic dechirp processing based pulse radar system is proposed and demonstrated. The dechirp processing is equivalent to use a RF coherent reference signal to mix with the transmitted LFM pulse. The key point of the equivalent dechirp processing is photonic mixing the echoes twice using an optical reference signal which is generated by a coherent IF-LFM signal with an equaled bandwidth and a doubled duration to the transmitted LFM pulse, so that the echoes reflected by a swath with a certain width are completely dechirp processed, and a constant range resolution implied by the transmitted bandwidth can be obtained over the swath. The enable techniques for equivalent dechirp processing are a PPDCR based detection scheme with a phase correlated optical reference signal and an algorithm to cancel the fiber phase noise caused by thermal fluctuations. The results of the optical delay line tests prove that the constant resolution of 6.7cm, which is close to the theoretical value, can be achieved along the width of the swath, while the results also show the ISLR can be improved by the phase noise cancellation algorithm. Finally, the proposed SAR system is evaluated by a rotating platform based ISAR imaging test. The photonic dechirp pulse SAR provides a promising solution for high resolution and long-range microwave imaging.

REFERENCES

[1] I. G. Cumming and F. H. Wong, "Synthetic aperture concepts," in *Digital Processing of Synthetic Aperture Radar Data: Algorithms and Implementation*. Norwood, MA, USA: Artech House, 2004, pp. 147–152.
[2] M. Skolnik, "Extraction of information and waveform design," in *Introduction to Radar Systems*, 3rd ed. New York, NY, USA: McGraw-Hill, 1980, pp. 399–438.
[3] J. Yao, "Microwave photonics," *J. Lightw. Technol.*, vol. 27, no. 3, pp. 314–335, Feb. 1, 2009.
[4] X. Zou, B. Lu, W. Pan, L. Yan, A. Stöhr, and J. Yao, "Photonics for microwave measurements," *Laser Photon. Rev.*, vol. 10, no. 5, pp. 711–734, Jul. 2016.
[5] P. Ghelfi, F. Laghezza, F. Scotti, G. Serafino, A. Capria, S. Pinna, D. Onori, C. Porzi, M. Scaffardi, A. Malacarne, V. Vercesi, E. Lazzeri, F. Berizzi, and A. Bogoni, "A fully photonics-based coherent radar system," *Nature*, vol. 507, no. 7492, pp. 341–345, Mar. 2014.
[6] R. Li, W. Li, M. Ding, Z. Wen, Y. Li, L. Zhou, S. Yu, T. Xing, B. Gao, Y. Luan, Y. Zhu, P. Guo, Y. Tian, and X. Liang, "Demonstration of a microwave photonic synthetic aperture radar based on photonic-assisted signal generation and stretch processing," *Opt. Exp.*, vol. 25, no. 13, pp. 14334–14340, Jun. 2017.
[7] F. Zhang, Q. Guo, Z. Wang, P. Zhou, G. Zhang, J. Sun, and S. Pan, "Photonics-based broadband radar for high resolution and real-time inverse synthetic aperture imaging," *Opt. Exp.*, vol. 25, no. 14, pp. 16274–16281, Jul. 2017.
[8] S. Wang, Z. Lu, N. Idrees, S. Zheng, X. Jin, X. Zhang, and X. Yu, "Photonic generation and de-chirping of broadband THz linear-frequency-modulated signals," *IEEE Photon. Technol. Lett.*, vol. 31, no. 11, pp. 881–884, Jun. 1, 2019.
[9] J. Fu, F. Zhang, D. Zhu, and S. Pan, "Fiber-distributed ultra-wideband radar network based on wavelength reusing transceivers," *Opt. Exp.*, vol. 26, no. 14, pp. 18457–18469, Jul. 2018.
[10] X. Zhang, H. Zeng, J. Yang, Z. Yin, Q. Sun, and W. Li, "Novel RF-source-free reconfigurable microwave photonic radar," *Opt. Exp.*, vol. 28, no. 9, pp. 13650–13661, Apr. 2020.
[11] W. J. Caputi, "Stretch: A time-transformation technique," *IEEE Trans. Aerosp. Electron. Syst.*, vol. AES-7, no. 2, pp. 269–278, Mar. 1971.
[12] W. H. Glenn, "Noise in interferometric optical systems: An optical Nyquist theorem," *IEEE J. Quantum Electron.*, vol. 25, no. 6, pp. 1218–1224, Jun. 1989.
[13] K. H. Wanser, "Fundamental phase noise limit in optical fibres due to temperature fluctuations," *Electron. Lett.*, vol. 28, no. 1, pp. 53–54, Jan. 1992.
[14] R. Li, X. Han, X. Chen, X. Chen, and J. Yao, "A phase-modulated microwave photonic link with an extended transmission distance," *IEEE Photon. Technol. Lett.*, vol. 27, no. 24, pp. 2563–2566, Dec. 15, 2015.
[15] J. Rodriguez and Y. Li, "Noise analysis for coherent phase-modulated RF fiber-optic link," *J. Lightw. Technol.*, vol. 39, no. 10, pp. 3072–3080, May 15, 2021.
[16] V. J. Urick, J. D. Mckinney, and K. J. Williams, "External intensity modulation with direct detection," in *Fundamentals of Microwave Photonics*. Hoboken, NJ, USA: Wiley, 2015, pp. 213–233.
[17] B. R. Mahafza, "Continuous wave (CW) radars," in *Radar Systems Analysis and Design Using MATLAB*. Boca Raton, FL, USA: CRC Press, 2013, pp. 64–68.
[18] M. Nakazawa, K. Kikuchi, and T. Miyazaki, "Coherent optical communications: Historical perspectives and future directions," in *High Spectral Density Optical Communication Technologies*. Berlin, Germany: Springer, 2010, pp. 26–28.
[19] *M8190A Arbitrary Waveform Generator User's Guide*, Keysight Technologies, Böblingen, Germany, 2015.
[20] I. G. Cumming and F. H. Wong, "Pulse compression of linear FM signals," in *Digital Processing of Synthetic Aperture Radar Data: Algorithms and Implementation*. Norwood, MA, USA: Artech House, 2004, pp. 80–87.

ZHENWEI MO received the B.E. degree from Chongqing University, Chongqing, China, in 2017. He is currently pursuing the Ph.D. degree with the National Key Laboratory of Microwave Imaging Technology, Aerospace Information Research Institute, Chinese Academy of Sciences, Beijing, China, and the School of Electronics, Electrical and Communication Engineering, University of Chinese Academy of Sciences, Beijing. His research interests include photonic microwave signal generation and processing.

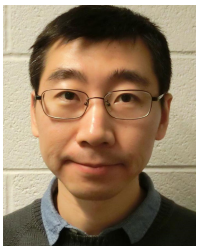

RUOMING LI (Senior Member, IEEE) received the Ph.D. degree in optical engineering from Nanjing University, Nanjing, China, in 2015. He was a Joint Training Student with the College of Engineering and Applied Sciences, Nanjing University, and the School of Electrical Engineering and Computer Science, University of Ottawa, Ottawa, ON, Canada. He currently works as an Associate Research Professor with the Aerospace Information Research Institute, Chinese Academy of Sciences. His current research interests include photonic-assisted microwave mixer, photonic-assisted synthetic aperture radar, photonic generation of microwave and millimeter-wave signals, and radio over fiber.

JIYAO YANG received the B.E. degree in electronic engineering from the Beijing Institute of Technology, Beijing, China, in 2016. He is currently pursuing the Ph.D. degree with the National Key Laboratory of Microwave Imaging Technology, Aerospace Information Research Institute, Chinese Academy of Sciences, Beijing, and the School of Electronics, Electrical and Communication Engineering, University of Chinese Academy of Sciences, Beijing. His research interests include microwave photonic radar and photonic channelization.

CHENYU LIU received the B.E. degree in information engineering from Shanghai Jiao Tong University, Shanghai, China, in 2018. He is currently pursuing the Ph.D. degree with the National Key Laboratory of Microwave Imaging Technology, Aerospace Information Research Institute, Chinese Academy of Sciences, Beijing, China, and the School of Electronics, Electrical and Communication Engineering, University of Chinese Academy of Sciences, Beijing. His research interests include microwave photonic radar and optical injection locking.

WANGZHE LI (Member, IEEE) received the B.E. degree in electronic science and technology from Xi'an Jiaotong University, Xi'an, China, in 2004, the M.Sc. degree in electrical engineering from Tsinghua University, Beijing, China, in 2007, and the Ph.D. degree in electrical engineering from the University of Ottawa, Ottawa, ON, Canada, in 2013. He is currently a Research Professor with the National Key Laboratory of Microwave Imaging Technology, Aerospace Information Research Institute, Chinese Academy of Sciences, Beijing. In 2018, he became the Director of the National Key Laboratory of Microwave Imaging Technology. His current research interests include photonic-assisted synthetic aperture radar, photonic generation of microwave and terahertz signals, arbitrary waveform generation, optoelectronic oscillation, and integrated photonics.